CHALMERS

Publication 00/2

LES-RANS of Channel Flow

Lars Davidson

Department of Thermo and Fluid Dynamics
CHALMERS UNIVERSITY OF TECHNOLOGY
Göteborg, Sweden, April 2000

LES-RANS of Channel Flow

Lars Davidson
Dept. of Thermo and Fluid Dynamics
Chalmers University of Technology
SE-412 96 Göteborg, Sweden
http://www.tfd.chalmers.se/~lada

Acknowledgment

This work was partly financed by the LESFOIL project in the Brite-Euram programme (project no. BE97-4483) .

1 Introduction

When Large Eddy Simulations are used very fine grids must be used in all three direction. In the wall-normal direction the near-wall grid spacing should be about $y^+ \simeq 1$, which is similar to the requirement in RANS. Contrary to RANS, in LES a fine grid should also be used in the spanwise (z) and streamwise (x) direction in order to resolve the near-wall turbulent processes (streaks), which are responsible for the major part of the turbulence production. The requirement for a well-resolved LES on Δx^+ and Δz^+ in the near-wall region is approximately 100 and 20, respectively [12]. In the fully turbulent region, say for $y^+ > 50$, coarser grid spacing can be used; Δx^+ and Δz^+ are in this region probably dictated by the requirement to resolve the time-averaged mean flow, rather than the near-wall turbulent processes.

In the present study, we propose to couple a two-equation $k-\omega$ model in the near-wall region (RANS region) with a one-equation k_{sgs} model in the core region (LES region). The momentum equation are solved throughout the computational domain. In the RANS region the turbulent viscosity from the $k-\omega$ model is used, and in the LES region the SGS viscosity from the one-equation model is used, see Fig. 1. For simplicity, the matching line is presently defined at a pre-selected grid line.

This approach is similar to the DES (Detached Eddy Simulation) [8, 13, 16, 17].

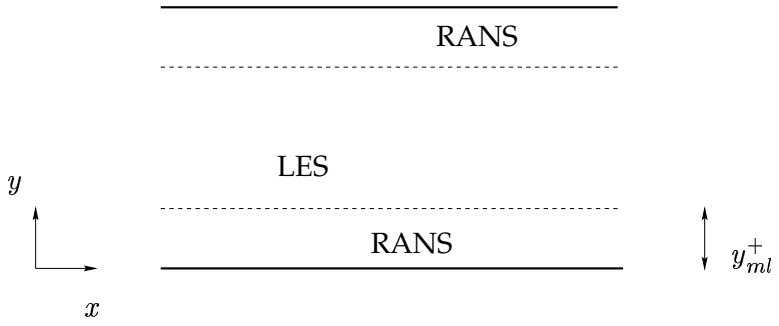

Figure 1: Configuration. The near-wall RANS region and the outer LES region.

2 Computational Details

An implicit, two-step time-advancement methods is used [5]. The Navier-Stokes equation for the $\bar{u}_i$ velocity reads

$$\frac{\partial \bar{u}_i}{\partial t} + \frac{\partial}{\partial x_j}\left(\bar{u}_i \bar{u}_j\right) = -\frac{1}{\rho}\frac{\partial \bar{p}}{\partial x_i} + \nu \frac{\partial^2 \bar{u}_i}{\partial x_j \partial x_j} - \frac{\partial \tau_{ij}}{\partial x_j} \tag{1}$$

When it is discretized it can be written

$$\begin{aligned} \bar{u}_i^{n+1} = \bar{u}_i^n + \Delta t H\left(\bar{u}_i^n, \bar{u}_i^{n+1}\right) - \frac{1}{\rho}\alpha \Delta t \frac{\partial \bar{p}^{n+1}}{\partial x_i} \\ - \frac{1}{\rho}(1-\alpha)\Delta t \frac{\partial \bar{p}^n}{\partial x_i} \end{aligned} \tag{2}$$

where $H\left(\bar{u}_i^n, \bar{u}_i^{n+1}\right)$ includes convection and the viscous and subgrid stresses, and $\alpha = 0.5$ (Crank-Nicholson). Second-order central differencing in space is used for all terms. Equation 2 is solved which gives $\bar{u}_i^{n+1}$ which does not satisfy continuity. An intermediate velocity field is computed by subtracting the implicit part of the pressure gradient, i.e.

$$\bar{u}_i^* = \bar{u}_i^{n+1} + \frac{1}{\rho}\alpha \Delta t \frac{\partial \bar{p}^{n+1}}{\partial x_i}. \tag{3}$$

Taking the divergence of Eq. 3 requiring that continuity (for the face velocities $\bar{u}_{i,f}^*$ which are obtained by linear interpolation) should be satisfied on level $n+1$, i.e. $\partial \bar{u}_{i,f}^{n+1}/\partial x_i = 0$ we obtain

$$\frac{\partial^2 \bar{p}^{n+1}}{\partial x_i \partial x_i} = \frac{\rho}{\Delta t \alpha}\frac{\partial \bar{u}_{i,f}^*}{\partial x_i}. \tag{4}$$

For more details, see Ref. [5, 14].

Case	x_{max}	z_{max}	m.l. y/δ	m.l. j_{match}	m.l. y^+	Δx^+	Δz^+	Δ
1	2π	0.5π	0.023	4	25	206	52	$(\Delta V)^{1/3}$
2	2π	0.5π	0.057	8	60	206	52	$(\Delta V)^{1/3}$
3	4π	π	0.023	4	25	412	104	$(\Delta V)^{1/3}$
4	4π	π	0.057	8	60	412	104	$(\Delta V)^{1/3}$
5	4π	π	0.057	8	60	412	104	Δy
6	4π	π	0	0	0	412	104	-

Table 1: Size of the computational domain and position of the matching line (m.l.) between the LES and RANS regions. The j_{match} value represents number of cells in the RANS region. Note that in Case 6 only LES is used.

Case	$\langle C_{hom} \rangle_t$
1	0.0065
2	0.0040
3	0.0084
4	0.0060
5	0.029
6	-

Table 2: Predicted value of the homogeneous coefficient (see Eq. 7).

3 Configuration

The flow in a channel is computed combining a one-equation k_{sgs} model of Davidson [3] with a two-equation $k-\omega$ model of Peng *et al.* [9]. The Reynolds number is $Re_\tau = u_\tau \delta/\nu = 1050$, where δ denotes the half-channel height. A mesh with $32 \times 64 \times 32$ (x, y, z) cells has been used. Different sizes of the computation domain have been used, see Table 1. The grid is refined near the walls using geometric stretching with an expansion factor of 1.10. The node adjacent to the walls is located at $y/\delta = 0.0025$ ($y^+ = 2.6$). The time step was set to $\Delta t = 0.0049$ ($u_\tau = 1$) which corresponds to a maximum convective CFL between 0.8 and 1. All results below have been time averaged during 3000 time steps, as well as averaged in the streamwise (x) and spanwise (z) directions.

4 LES–RANS model

In the near-wall layer a $k-\omega$ model is used, and in the core region a dynamic one-equation SGS model is used. The $k-\omega$ model reads [9]

$$\begin{aligned}
&\frac{\partial k}{\partial t}+\frac{\partial}{\partial x_j}(U_j k)=\frac{\partial}{\partial x_j}\left[\left(\nu+\frac{\nu_t}{\sigma_k}\right)\frac{\partial k}{\partial x_j}\right]+P_k-c_k f_k \omega k\\
&\frac{\partial \omega}{\partial t}+\frac{\partial}{\partial x_j}(U_j \omega)=\left[\left(\nu+\frac{\nu_t}{\sigma_\omega}\right)\frac{\partial \omega}{\partial x_j}\right]+\frac{\omega}{k}\left(c_{\omega 1} f_\omega P_k-c_{\omega 2}k\omega\right)+c_\omega\frac{\nu_t}{k}\left(\frac{\partial k}{\partial x_j}\frac{\partial \omega}{\partial x_j}\right)\\
&\qquad \nu_t=f_\mu\frac{k}{\omega},\ f_k=1-0.722\exp\left[-\left(\frac{R_t}{10}\right)^4\right]\\
&\qquad f_\mu=0.025+\left\{1-\exp\left[-\left(\frac{R_t}{10}\right)^{3/4}\right]\right\}\\
&\qquad\quad \left\{0.975+\frac{0.001}{R_t}\exp\left[-\left(\frac{R_t}{200}\right)^2\right]\right\}\\
&\qquad f_\omega=1+4.3\exp\left[-\left(\frac{R_t}{1.5}\right)^{1/2}\right],\ f_\omega=1+4.3\exp\left[-\left(\frac{R_t}{1.5}\right)^{1/2}\right]\\
&\qquad c_k=0.09,\ c_{\omega 1}=0.42,\ c_{\omega 2}=0.075\\
&\qquad c_\omega=0.75, \sigma_k=0.8,\ \sigma_\omega=1.35
\end{aligned} \tag{5}$$

The one-equation model employed in the LES region reads [3]

$$\begin{aligned}
\frac{\partial k_{sgs}}{\partial t}+\frac{\partial}{\partial x_j}(\bar{u}_j k_{sgs})&=\frac{\partial}{\partial x_j}\left[(\nu+\nu_t)\frac{\partial k_{sgs}}{\partial x_j}\right]+P_{k_{sgs}}-C_*\frac{k_{sgs}^{\frac{3}{2}}}{\Delta}\\
P_{k_{sgs}}&=2C\Delta k_{sgs}^{\frac{1}{2}}\bar{S}_{ij}\bar{S}_{ij}\\
\nu_t&=C_{hom}\Delta k_{sgs}^{\frac{1}{2}}\\
\Delta&=(\delta V)^{1/3}
\end{aligned} \tag{6}$$

The coefficients in the production term C and the dissipation term C_* are computed dynamically, using similarity between the turbulence at the grid filter and the test filter. The turbulent viscosity ν_t is used in the momentum equations, and the homogeneous C_{hom} is computed from the requirement that it should give the same production $\langle P_{k_{sgs}}\rangle_{xyz}$ (volume-averaged in the domain) as C, i.e.

$$\langle 2C\Delta k_{sgs}^{\frac{1}{2}}\bar{S}_{ij}\bar{S}_{ij}\rangle_{xyz}=2C_{hom}\langle\Delta k_{sgs}^{\frac{1}{2}}\bar{S}_{ij}\bar{S}_{ij}\rangle_{xyz} \tag{7}$$

For more details, see Refs. [3, 4, 6, 15].

The matching line near the lower wall is located at y_{ml}, see Table 1 and Fig. 1. Let's j_{match} denote the cell below the matching line y_{ml}. At the

matching line the following boundary conditions are used.

$$
\begin{aligned}
&j = j_{match}: \ \frac{\partial k}{\partial y} = \frac{\partial \omega}{\partial y} = 0 \\
&j = j_{match}+1: \ \nu_{sgs,j_{match}+1} = \nu_{t,j_{match}} \ \Rightarrow k^{-}_{sgs} = \left(\frac{\nu_t}{C_{hom}\Delta}\right)^2_{j_{match}}.
\end{aligned}
\tag{8}
$$

k^{-}_{sgs} is the SGS kinetic energy which is transported by convection-diffusion over the matching line from the RANS region to the LES region. At the upper matching line, the boundary conditions are of course the same. In finite volume context, this boundary condition is implemented as follows. The finite volume equations for all transport equations are written as (for simplicity we present the equation in 1D)

$$
\begin{aligned}
a_P\Phi_P &= a_N\Phi_N + a_S\Phi_S + S_U \\
a_P &= a_N + a_S - S_P
\end{aligned}
\tag{9}
$$

where Φ is k_{sgs} or ω. Let's write the above equation for the first j node above the lower matching line ($j = j_{match}+1$), see Fig.1. We introduce the "boundary condition" from the matching line (south neighbor) via source terms, i.e.

$$
S_U = a_S k^{-}_{sgs}, \ S_P = -a_S \tag{10}
$$

where a_S includes the usual convection and diffusion part. After that, we cut off the usual convection-diffusion contribution from the south neighbor by setting $a_S = 0$.

The same discretized momentum equations (Eq. 1) are solved in the entire computational domain, but different turbulent viscosities are used in the two regions. In the RANS region the turbulent viscosity from the $k-\omega$ model is used, and in the LES region the SGS viscosity from the one-equation model is used. This implies that in the RANS region we are doing unsteady RANS, i.e. the dependent variables $\bar{u}_i$, $\bar{p}$ etc. are time-averaged rather than filtered. Formally the time averaging interval ΔT in

$$
U(x_i,t) \equiv \bar{u}(x_i,t) = \frac{1}{2\Delta T}\int_{-\Delta T}^{\Delta T} u(x_i,t')dt' \tag{11}
$$

should be much smaller than the time scale of U. This condition is probably not satisfied.

The k and ω equations are discretized using Crank-Nicolson in time. In space central differencing is employed for all terms except for the convection terms, for which hybrid central/upwind differencing is used.

5 Results

The present RANS-LES model gives very good results for Case 1 & 2 (small Δx and Δz), see Figs. 2 and 3. When the resolution is made coarser (Figs. 4

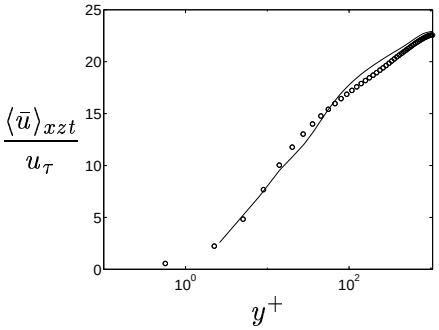

(a) $\bar{u}$ velocity.

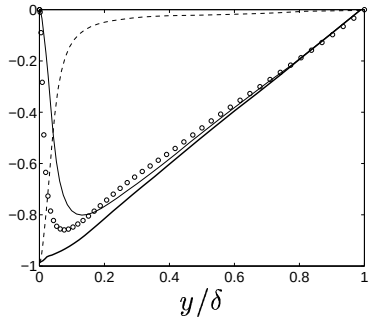

(b) Shear stresses. Thin solid line: resolved shear stress; dashed line: viscous plus eddy viscosity shear stress; thick solid line: total shear stress.

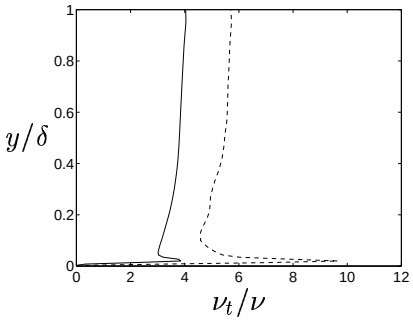

(c) SGS (or RANS) eddy viscosity. Solid line: time-averaged viscosity; dashed line: maximum eddy viscosity during averaging in time, x and z direction.

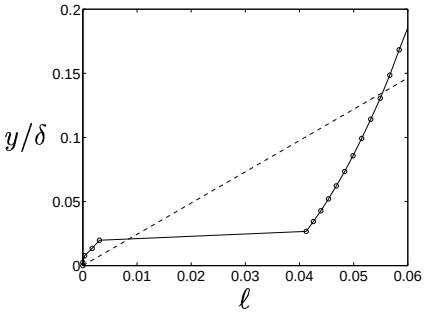

(d) Turbulent length scale. Solid line: RANS length scale $\ell = c_\mu^{-0.25}\nu_t k^{-1/2}$ and LES filter width $\ell = \Delta = (\Delta x \Delta y \Delta z)^{1/3}$; dashed line: $0.41y$. Markers show location of grid nodes.

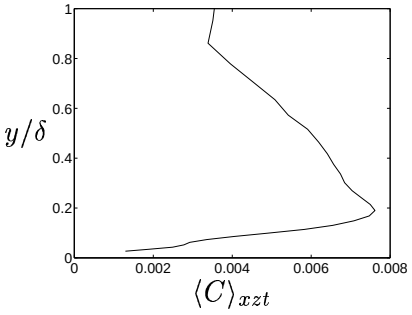

(e) Dynamic coefficient C.

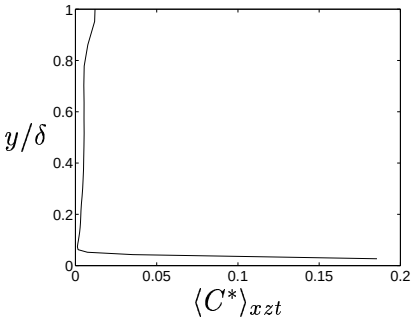

(f) Dynamic coefficient C_*.

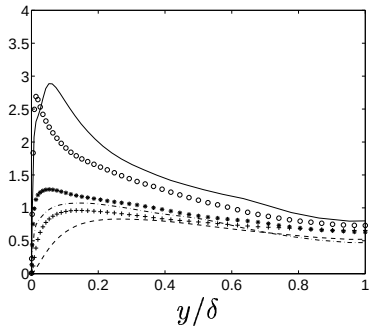

(g) Resolved stresses.

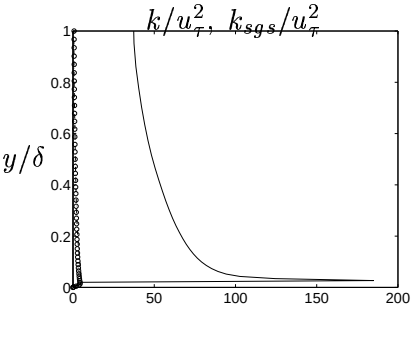

(h) Kinetic energies. Solid line: k_{sgs} or k.

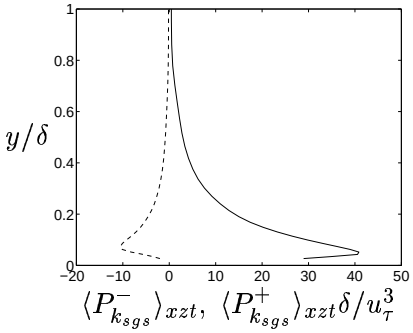

(i) Positive (solid line) and negative (dashed line) production.

Figure 2: Markers: LES by Piomelli [10]. Case 1.

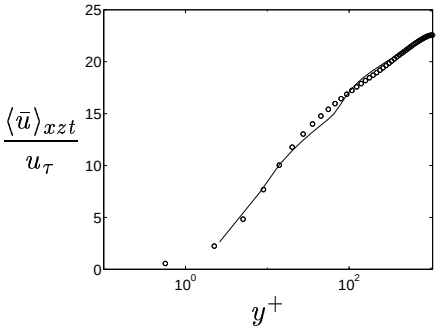

(a) $\bar{u}$ velocity.

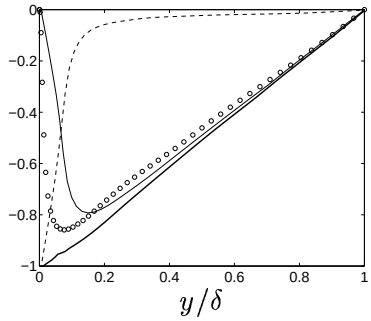

(b) Shear stresses. Thin solid line: resolved shear stress; dashed line: viscous plus eddy viscosity shear stress; thick solid line: total shear stress.

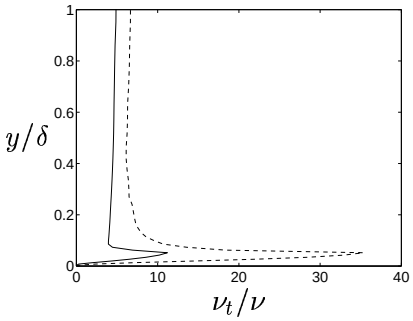

(c) SGS (or RANS) eddy viscosity. Solid line: time-averaged viscosity; dashed line: maximum eddy viscosity during averaging in time, x and z direction.

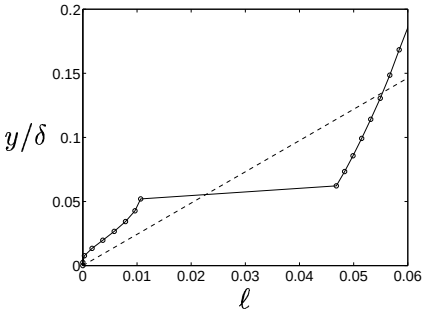

(d) Turbulent length scale. Solid line: RANS length scale $\ell = c_\mu^{-0.25} \nu_t k^{-0.5}$ and LES filter width $\ell = \Delta = (\Delta x \Delta y \Delta z)^{1/3}$; dashed line: $0.41y$. Markers show location of grid nodes.

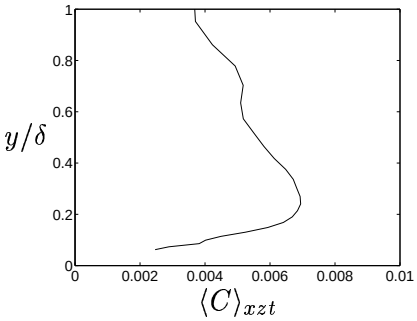

(e) Dynamic coefficient C.

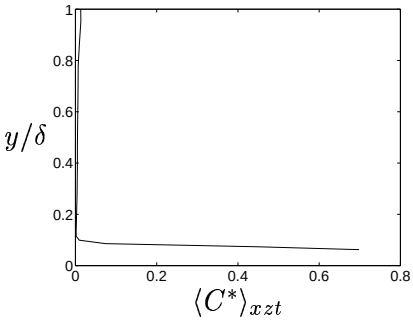

(f) Dynamic coefficient C_*.

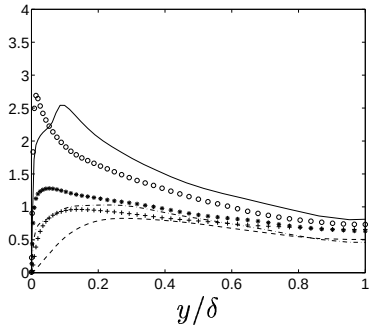

(g) Resolved stresses.

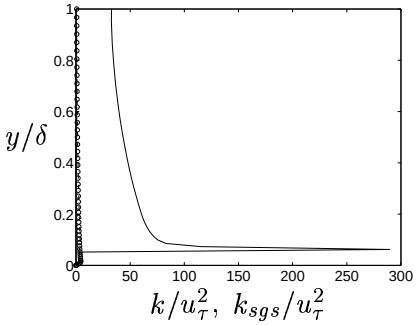

(h) Kinetic energies. Solid line: k_{sgs} or k.

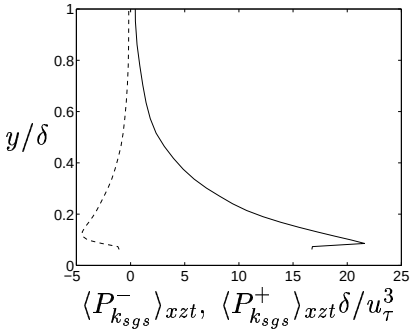

(i) Positive (solid line) and negative (dashed line) production.

Figure 3: Markers: LES by Piomelli [10]. Case 2.

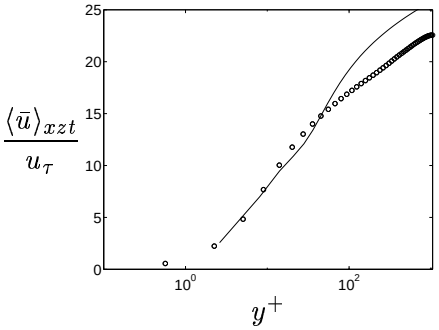

(a) $\bar{u}$ velocity.

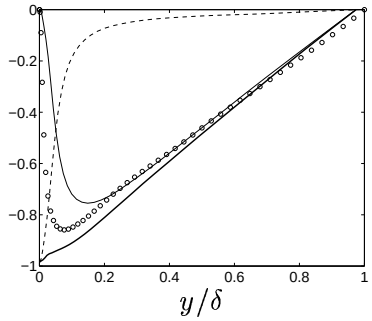

(b) Shear stresses. Thin solid line: resolved shear stress; dashed line: viscous plus eddy viscosity shear stress; thick solid line: total shear stress.

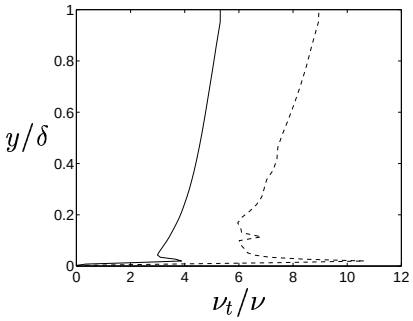

(c) SGS (or RANS) eddy viscosity. Solid line: time-averaged viscosity; dashed line: maximum eddy viscosity during averaging in time, x and z direction.

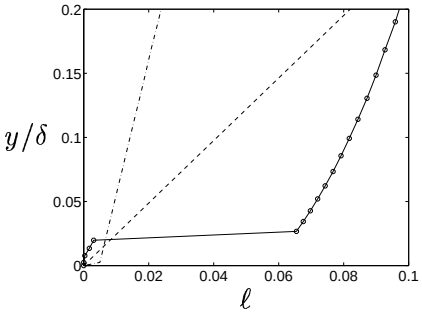

(d) Turbulent length scale. Solid line: RANS length scale $\ell = c_\mu^{-0.25} \nu_t k^{-1/2}$ and LES filter width $\ell = \Delta = (\Delta x \Delta y \Delta z)^{1/3}$; dashed line: $0.41y$; dash-dotted line: Δy. Markers show location of grid nodes.

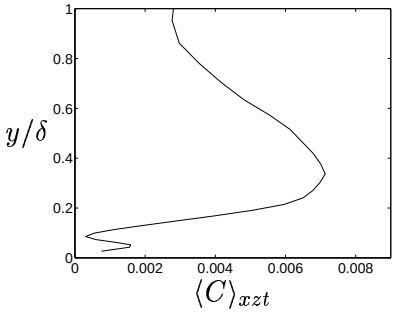

(e) Dynamic coefficient C.

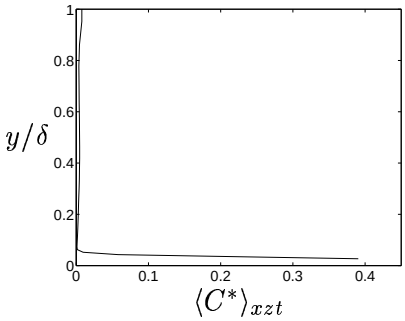

(f) Dynamic coefficient C_*.

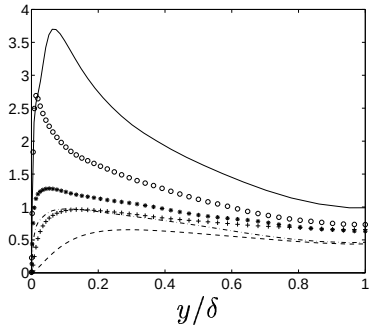

(g) Resolved stresses.

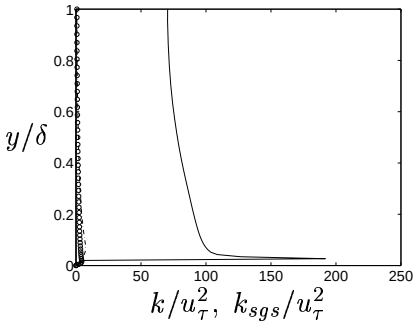

(h) Kinetic energies. Solid line: k_{sgs} or k.

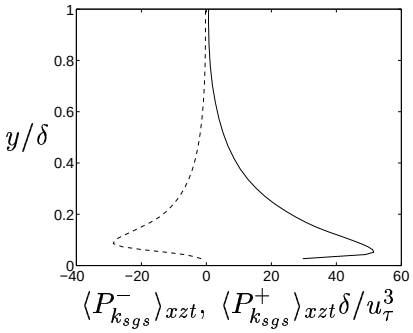

(i) Positive (solid line) and negative (dashed line) production.

Figure 4: Markers: LES by Piomelli [10]. Case 3.

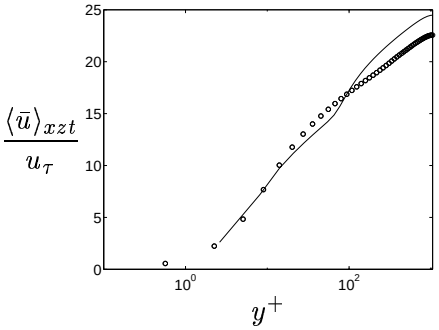

(a) $\bar{u}$ velocity.

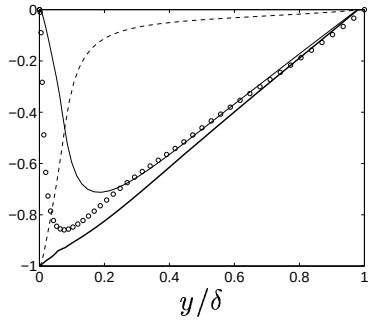

(b) Shear stresses. Thin solid line: resolved shear stress; dashed line: viscous plus eddy viscosity shear stress; thick solid line: total shear stress.

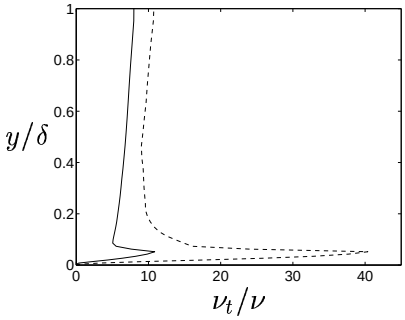

(c) SGS (or RANS) eddy viscosity. Solid line: time-averaged viscosity; dashed line: maximum eddy viscosity during averaging in time, x and z direction.

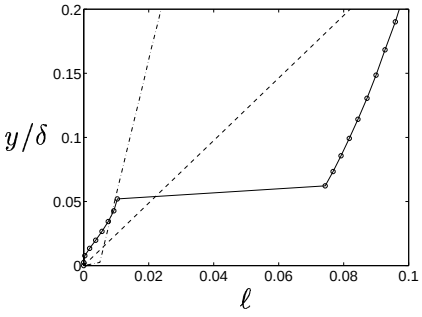

(d) Turbulent length scale. Solid line: RANS length scale $\ell = c_\mu^{-0.25}\nu_t k^{-1/2}$ and LES filter width $\ell = \Delta = (\Delta x \Delta y \Delta z)^{1/3}$; dashed line: $0.41y$; dash-dotted line: Δy. Markers show location of grid nodes.

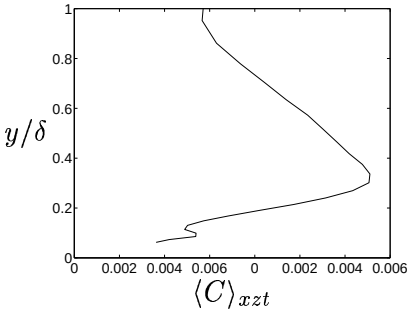

(e) Dynamic coefficient C.

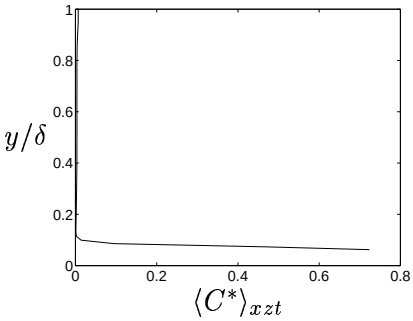

(f) Dynamic coefficient C_*.

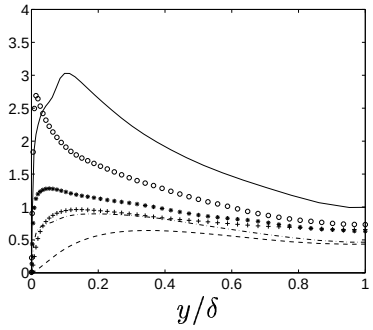

(g) Resolved stresses.

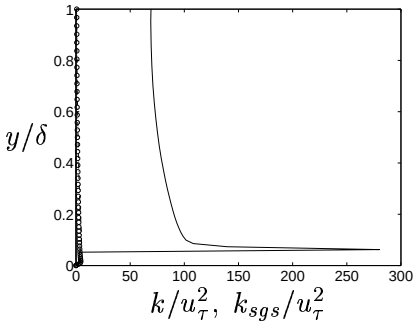

(h) Kinetic energies. Solid line: k_{sgs} or k.

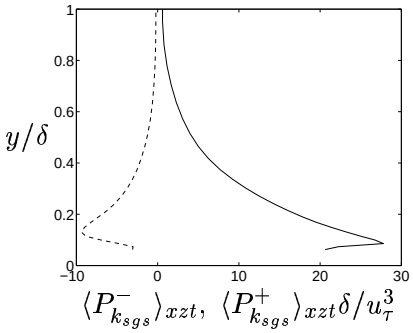

(i) Positive (solid line) and negative (dashed line) production.

Figure 5: Markers: LES by Piomelli [10]. Case 4.

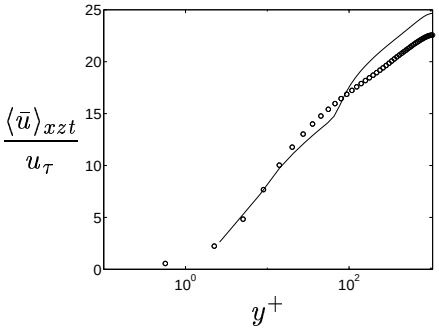

(a) $\bar{u}$ velocity.

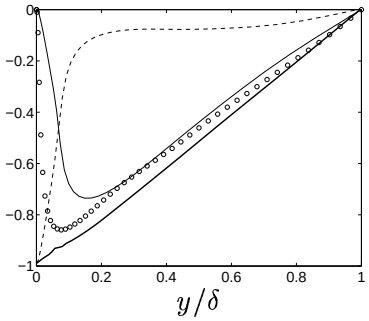

(b) Shear stresses. Thin solid line: resolved shear stress; dashed line: viscous plus eddy viscosity shear stress; thick solid line: total shear stress.

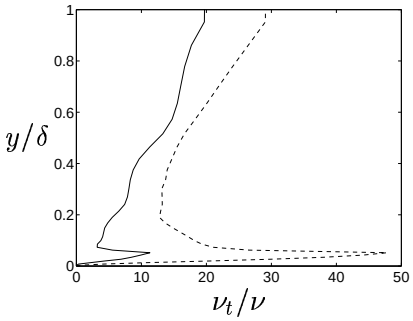

(c) SGS (or RANS) eddy viscosity. Solid line: time-averaged viscosity; dashed line: maximum eddy viscosity during averaging in time, x and z direction.

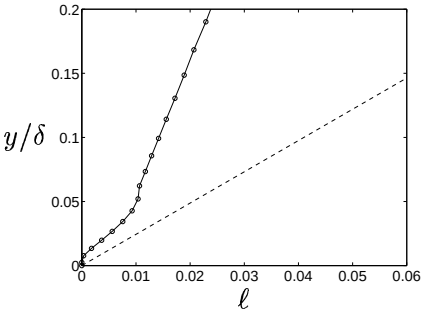

(d) Turbulent length scale. Solid line: RANS length scale $\ell = c_\mu^{-0.25}\nu_t k^{-1/2}$ and LES filter width $\ell = \Delta = \Delta y$; dashed line: $0.41y$. Markers show location of grid nodes.

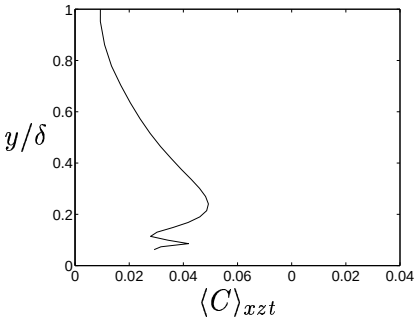

(e) Dynamic coefficient C.

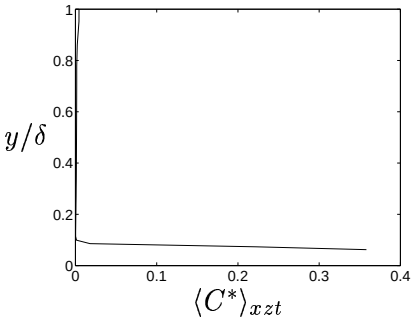

(f) Dynamic coefficient C_*.

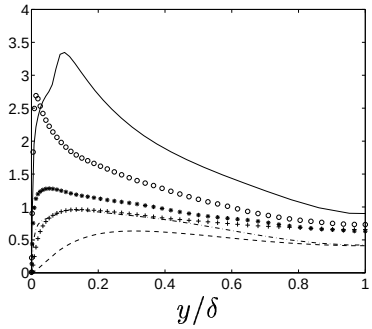

(g) Resolved stresses.

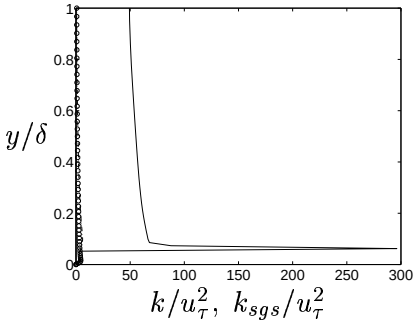

(h) Kinetic energies. Solid line: k_{sgs} or k.

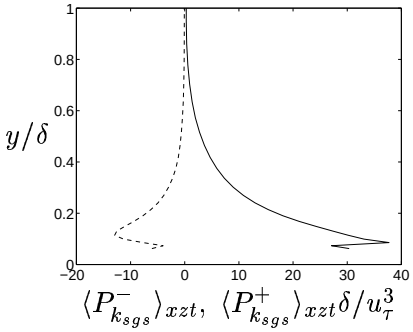

(i) Positive (solid line) and negative (dashed line) production.

Figure 6: Markers: LES by Piomelli [10]. Case 5.

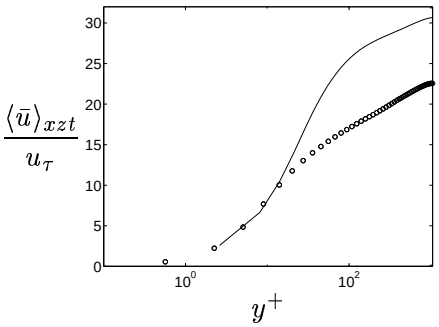

(a) $\bar{u}$ velocity.

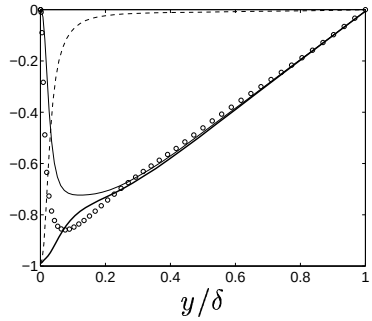

(b) Shear stresses. Thin solid line: resolved shear stress; dashed line: viscous plus eddy viscosity shear stress; thick solid line: total shear stress.

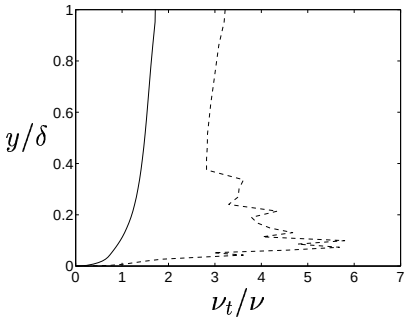

(c) SGS (or RANS) eddy viscosity. Solid line: time-averaged viscosity; dashed line: maximum eddy viscosity during averaging in time, x and z direction.

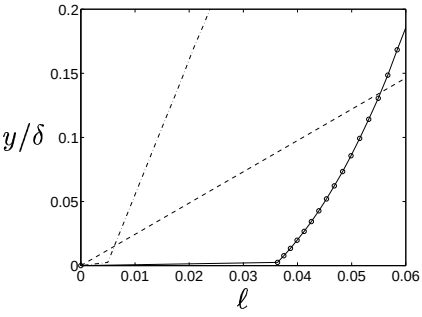

(d) Turbulent length scale. Solid line: LES filter width $\ell = \Delta = (\Delta x \Delta y \Delta z)^{1/3}$; dashed line: $0.41y$; dash-dotted line: Δy. Markers show location of grid nodes.

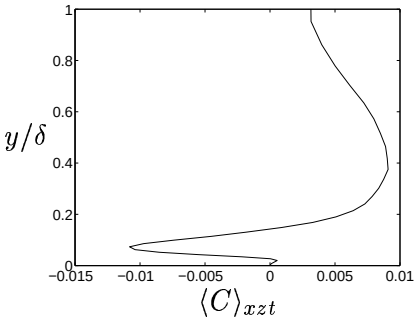

(e) Dynamic coefficient C.

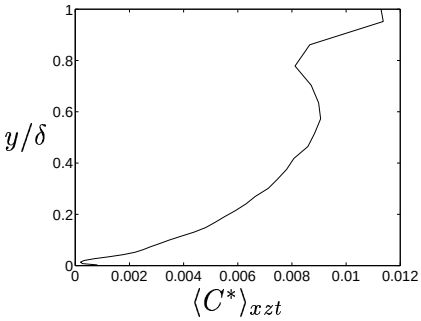

(f) Dynamic coefficient C_*.

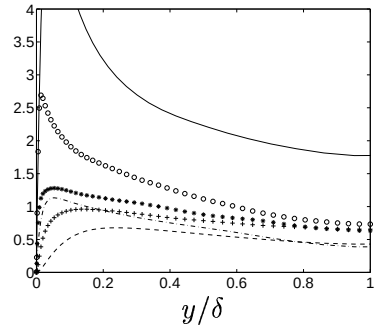

(g) Resolved stresses.

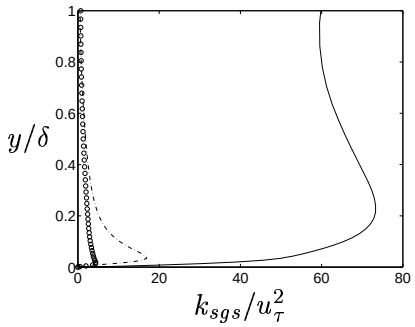

(h) Kinetic energies. Solid line: k_{sgs}.

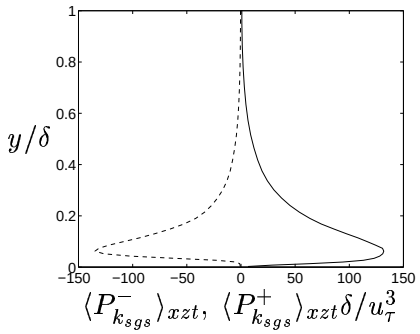

(i) Positive (solid line) and negative (dashed line) production.

Figure 7: Markers: LES by Piomelli [10]. Case 6 Note change of scale in a) compared to Figs. 2-6.

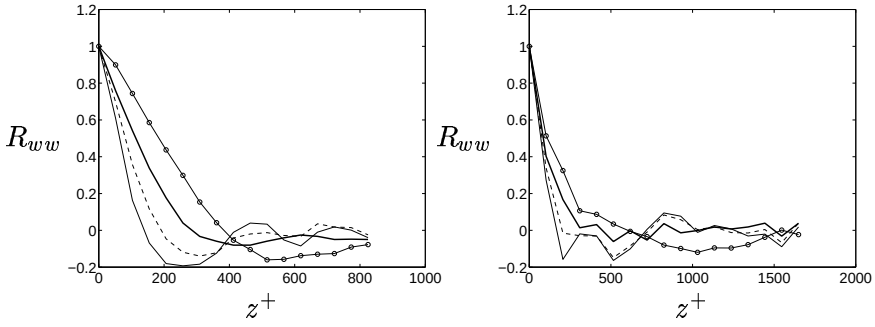

(a) Case 1.

(b) Case 2.

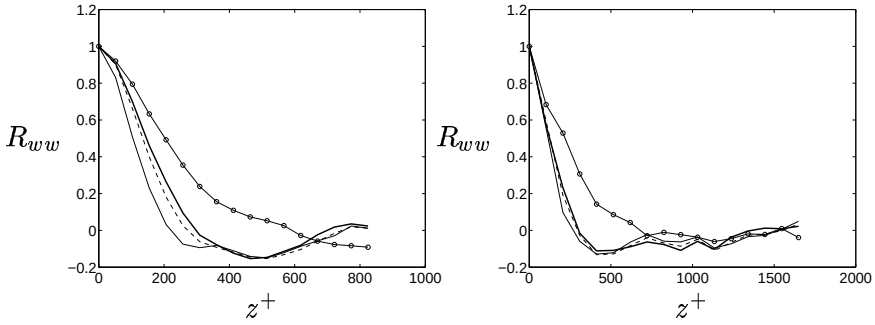

(c) Case 3.

(d) Case 4.

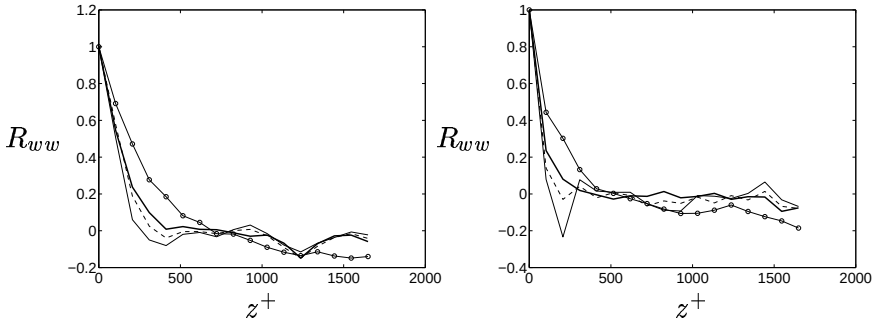

(e) Case 5.

(f) Case 6.

Figure 8: Resolved two-point correlations $R_{ww}(z)$. Thin solid line: $y^+ = 10$ (node 3); dashed line: $y^+ = 30$ (node 7); thick solid line: $y^+ = 116$ (node 11); thin solid line with circles: $y^+ = 220$ (node 20). Node 1 is the wall node.

and 5) the agreement with benchmark LES gets somewhat worse. It can also be seen a small jump appears in the velocity profiles. However, the RANS-LES model gives much better agreement compared with when only LES is used, see Fig. 7.

The SGS/RANS contribution to the total shear stress is seen, as expected, to increase when the resolution is made coarser or when the matching line is moved away from the wall, see Figs. 2(b)-5(b). This can also be seen from the SGS/RANS viscosity ν_t/ν, see Figs. 2(c)-5(c). It should be noted that the resolved stresses in the RANS region are large. This implies that the RANS region is affected to a large extent by the LES region, since the resolved turbulence in the LES region propagates down into the RANS region.

It is interesting to study the turbulent length scale. In the RANS region it is not in general clear how to express the velocity scale $\mathcal{U}$ and the length scale ℓ. However, in the logarithmic region the velocity scale should be u_τ and the length scale κy, i.e.

$$\nu_t = \mathcal{U}\ell = \kappa u_\tau y. \tag{12}$$

Furthermore, in the logarithmic region we have $k = c_\mu^{-1/2} u_\tau^2$ ($c_\mu = 0.09$), so that (see Eq. 5)

$$\nu_t = f_\mu k^{1/2} c_\mu^{-1/4} u_\tau/\omega \Rightarrow \ell = f_\mu k^{1/2} c_\mu^{-1/4}/\omega = c_\mu^{-1/4} \nu_t k^{-1/2}. \tag{13}$$

In Figs. 2(d)- 5(d) the length scale is presented. It can be seen that there is a jump in ℓ over the interface. What, at first, is somewhat surprising is that the LES length scale is *larger* than the RANS length scale. However, keeping in mind that $\Delta x \gg \Delta y$ and $\Delta z \gg \Delta y$, it is clear that this should be the case in an attached boundary layer. In Fig. 6, predictions are presented employing a different definition of the filter width (see Table 1)

$$\Delta = \min\{\Delta x, \Delta y, \Delta z\} \equiv \Delta y \tag{14}$$

Comparing Figs. 5 ($\Delta = (\delta V)^{1/3}$) and 6 ($\Delta = \Delta y$) we can see that the velocity profiles (a) and the resolved stresses [(b) and (g)] are very similar. The reason is that the dynamic coefficients have adjusted to the new definition of the filter width, see Figs. 5(e),(f) and 6(e),(f) and Table 2. To compensate for the decreased magnitude of Δ the dynamic coefficient C increases (e) and the coefficient in front of the dissipation term decreases (f); the homogeneous coefficient $\langle C_{hom} \rangle_t$ increases from 0.0060 to 0.028 (Table 2). There are also some differences between Figs. 5 and 6: the SGS viscosity in the core region is larger in the latter case. The length scale in Fig. 6(d) is fairly continuous across the matching line.

The interface condition in Eq. 8 enforces a continuous RANS/SGS viscosity, although the gradient of ν_t in the interface region is large. The large gradient is due to two factors. First (the main reason), the coefficient in the expression for ν_t in Eq. 5 (RANS region) is much larger than that in the expression for ν_t in Eq. 6 (LES region). Second, the coefficients in the source

term in the k equation are very different in the RANS region and in the LES region. The coefficient in the expression for ν_t changes instantaneously over the matching line, whereas the change in the source term in the k_{sgs} equation progressively, via convection and diffusion, decreases the turbulent SGS kinetic energy in the LES region as the distance from the interface increases. One way to achieve a smoother variation of ν_t in the interface region would be to make the coefficient in the expression of ν_t in the LES region and the RANS region more equal. On the other hand, this would alter the LES model and could make it less appropriate for modelling the SGS stresses in the LES region.

As can be seen in Figs. 2(h)- 6(h), the kinetic energy is *very* large in the LES region. This is because of the interface condition (Eq. 8) which gives a very large k_{sgs}^{-}. Thus $(k_{sgs})^{1/2}$ is not a relevant velocity scale for the SGS fluctuations. A relevant velocity scale for the SGS fluctuations would probably be $C_{hom}(k_{sgs})^{1/2}$. However, the only important quantity coming out from the SGS model (the dynamic one-equation model) is the SGS viscosity, and this quantity appears to have a reasonable magnitude, see Figs. 2(c)- 6(c).

As can be seen, k_{sgs} is very large also in Fig. 7 (only LES). This is because of the coarse grid. For a grid with good resolution ($\Delta z^+ = 38$, $\Delta x^+ = 76$), the k_{sgs} is indeed smaller than the resolved kinetic energy [2, 7].

The production, $P_{k_{sgs}}$, is shown in Figs. 2(i)- 7(i). It has been split into one positive part and one negative part according to [11]

$$\begin{aligned} P^+ &= \frac{1}{2}\left(P_{k_{sgs}} + |P_{k_{sgs}}|\right) \\ P^- &= \frac{1}{2}\left(P_{k_{sgs}} - |P_{k_{sgs}}|\right). \end{aligned} \tag{15}$$

It can be seen that part of the production is negative (backscatter), thereby reducing the total production, and thereby also k_{sgs} and ν_{sgs}. It should be remembered that, in the dynamic Germano model, only very small magnitudes of negative ν_{sgs} are permitted, but that the magnitude of negative ν_{sgs} is not limited in any way in the dynamic one-equation SGS model. Furthermore, it can be seen that the net production increases for decreasing resolution (decreasing Δx^+ and Δz^+), which is one of the reasons why ν_{sgs} increases for decreasing resolution. When LES is used in the entire computational domain (Case 6), it can be seen that the magnitude of the negative production is actually larger than the positive part (see Fig. 7(i)). This is a result of the poor resolution. With an appropriate resolution, the net production is, as it should, positive [2, 7].

In Fig. 8 the two-point correlation R_{ww} is presented. It is defined as

$$R_{ww}(z) = \frac{\langle w'(z_0)w'(z-z_0)\rangle_{xt}}{w'^2_{rms}(z_0)} \tag{16}$$

where w' is resolved spanwise flucatuation and z_0 is the spanwise midpoint of the channel, i.e. $z_0 = z_{max}$. In a wall-resolved LES, the minimum in R_{ww}

should indicate half the mean distance between the streamwise streaks. As mentioned in the introduction, we do not expect to resolve these streaks in a physical correct way. However, Baggett [1] reports unphysical spanwise correlations whose width were dictated by the cell size Δz. For Case 2 & 6, which are cases with poor resolution and a thin RANS region (see Table 1), R_{ww} exhibit minima at $\Delta z^+ \simeq 200$, which corresponds to $2\Delta z$. However, the sharp minima in R_{ww} disappear when the thickness of the RANS region is increased. The fact that the unphysical minima do not show up for the cases in which the RANS region is thick, indicates that the RANS model near the wall is modelling the turbulence as intended, rather than trying to resolve it.

6 Conclusions

A hybrid LES-RANS model has been proposed. Fairly good results have been presented for channel flow at $Re_\tau = 1050$. At the interface region between the RANS and the LES region, large gradients of ν_t prevail. This results in a small jump in the velocity profile over the interface. Some improvements in the interface region are probably needed.

The resolved spanwise correlations indicate unphysical streaks close to the wall, whose spacing seem to be dictated by the spanwise grid spacing. However, when the thickness of the RANS region is increased, these unphysical streaks disappear. This indicates that the thickness of the RANS region should not be too thin.

References

[1] BAGGETT, J. On the feasibility of merging LES with RANS for the near-wall region of attached turbulent flows. In *Annual Research Briefs* (Center for Turbulent Research, Stanford Univ./NASA Ames Reseach Center, 1998), pp. 267–278.

[2] DAHLSTRÖM, S., AND DAVIDSON, L. Chalmers' 12-month report, LESFOIL: A Brite-Euram project. Tech. rep., Dept. of Thermo and Fluid Dynamics, Chalmers University of Technology, Gothenburg, 1999.

[3] DAVIDSON, L. Large eddy simulation: A dynamic one-equation subgrid model for three-dimensional recirculating flow. In *11th Int. Symp. on Turbulent Shear Flow* (Grenoble, 1997), vol. 3, pp. 26.1–26.6.

[4] DAVIDSON, L. Large eddy simulations: A note on derivation of the equations for the subgrid turbulent kinetic energies. Tech. Rep. 97/11, Dept. of Thermo and Fluid Dynamics, Chalmers University of Technology, Gothenburg, 1997.

[5] DAVIDSON, L. LES of recirculating flow without any homogeneous direction: A dynamic one-equation subgrid model. In *2nd Int. Symp. on Turbulence Heat and Mass Transfer* (Delft, 1997), K. Hanjalić and T. Peeters, Eds., Delft University Press, pp. 481–490.

[6] KRAJNOVIĆ, S. Large eddy simulation of the flow around a three-dimensional bluff body. Thesis for Licentiate of Engineering 00/1, Dept. of Thermo and Fluid Dynamics, Chalmers University of Technology, Gothenburg, Sweden, January 2000.

[7] KRAJNOVIĆ, S., AND DAVIDSON, L. Large-eddy simulation of the flow around a surface-mounted cube using a dynamic one-equation subgrid model. In *The First International Symp. on Turbulence and Shear Flow Phenomena* (New York, 1999), S. Banerjee and J. Eaton, Eds., begell house, inc., pp. 741–746.

[8] NIKITON, N., NICOUD, F., WASISTHO, B., SQUIRES, K., AND SPALART, P. An approach to wall modeling in large-eddy simulations (submitted for publication).

[9] PENG, S.-H., DAVIDSON, L., AND HOLMBERG, S. A modified Low-Reynolds-Number $k-\omega$ model for recirculating flows. *ASME: Journal of Fluids Engineering 119* (1997), 867–875.

[10] PIOMELLI, U. High Reynolds number calculations using the dynamic subgrid-scale stress model. *Physics of Fluids A 5* (1993), 1484–1490.

[11] PIOMELLI, U., CABOT, W., MOIN, P., AND LEE, S. Subgrid-scale backscatter in turbulent and transitional flows. *Physics of Fluids A 3* (1991), 1766–1771.

[12] PIOMELLI, U., AND CHASNOV, J. Large-eddy simulations: Theory and applications. In *Transition and Turbulence Modelling* (Dordrecht, 1996), D. Henningson, M. Hallbaeck, H. Alfreddson, and A. Johansson, Eds., Kluwer Academic Publishers, pp. 269–336.

[13] SHUR, M., SPALART, P., STRELETS, M., AND TRAVIN, A. Detached-eddy simulation on an airfoil at high angle of attack. In *Engineering Turbulence Modelling and Experiments 4* (1999), W. Rodi and D. Laurence, Eds., Elsevier, pp. 669–678.

[14] SOHANKAR, A. *Numerical Study of Laminar, Transitional and Turbulent Flow Past Rectangular Cylinders*. PhD thesis, Dept. of Thermo and Fluid Dynamics, Chalmers University of Technology, Gothenburg, 1998.

[15] SOHANKAR, A., DAVIDSON, L., AND NORBERG, C. Large eddy simulation of flow past a square cylinder: Comparison of different subgrid scale models. *ASME: Journal of Fluids Engineering 122*, 1 (2000), 39–47.

[16] SPALART, P., JOU, W.-H., M.STRELETS, AND ALLMARAS, S. Comments on the feasability of LES for wings and on a hybrid RANS/LES approach. In *Advances in LES/DNS, First Int. conf. on DNS/LES* (Louisiana Tech University, 1997), C. Liu and Z. Liu, Eds., Greyden Press.

[17] TRAVIN, A., SHUR, M., STRELETS, M., AND SPALART, P. Detached-eddy simulations past a circular cylinder (submitted for publication).